Geophysical Research Letters

RESEARCH LETTER
10.1029/2019GL085958

# Equipotential Figure of Phobos Suggests Its Late Accretion Near 3.3 Mars Radii

**Xuanyu Hu[1], Jürgen Oberst[1,2], and Konrad Willner[2]**

[1]Institute of Geodesy and Geoinformation Science, Technical University Berlin, Berlin, Germany, [2]Institute of Planetary Research, German Aerospace Center (DLR), Berlin, Germany

**Key Points:**
- We determined surface heights of Phobos relative to its normal, equipotential ellipsoid
- Height statistics indicate Phobos would be nearly equipotential at 3.3 Mars radii
- Results support that Phobos was accreted from a debris ring after a previous tidal disruption

**Supporting Information:**
- Supporting Information S1

**Correspondence to:**
X. Hu,
xuanyuhu@gmail.com

**Citation:**
Hu, X., Oberst, J., & Willner, K. (2020). Equipotential figure of phobos suggests its late accretion near 3.3 Mars radii. *Geophysical Research Letters*, *47*, e2019GL085958. https://doi.org/10.1029/2019GL085958

Received 23 OCT 2019
Accepted 28 JAN 2020
Accepted article online 3 FEB 2020

**Abstract** The ellipsoidal figure of Phobos has been tentatively interpreted as resulting from accretion in a tidal environment close to its parent planet Mars. The issue is compounded by the rapid tidal decay of the moon's orbit. Consequently, when and where the moon actually formed remains elusive. We determined the gravity equipotential ellipsoid of Phobos during its orbital decay and studied the evolution of surface ellipsoidal heights. We found that the equipotential ellipsoid closely fits the body shape near 3.6 Mars radii. Meanwhile, the height distribution resembles Gaussian at 3.3 Mars radii, suggesting equilibrium of topography. The ellipsoidal shape may have accreted here under appreciable tidal influence of roughly half the magnitude at Phobos' current position (at 2.76 Mars radii). This lends evidential support to the hypothesis that Phobos is not a primordial object but has reaccreted from a debris ring after a previous disruption event.

## 1. Introduction

There is an ongoing debate on whether Phobos and Deimos were captured extraneous objects or formed in situ from a circumplanetary disk (Burns, 1992; Lambeck, 1979; Peale, 1999). The former hypothesis hinges on the observed morphological and spectroscopic similarities of the moons to carbonaceous chondritic objects amply found in the Main asteroid belt. The evidence is far from conclusive (Pieters et al., 2014). A persistent difficulty with the capture scenario is to explain the evolution of the initially probably eccentric orbits near the ecliptic to the present-day near-circular orbits almost within the Martian equatorial plane. For Phobos, tidal dissipation yields a viable mechanism for the circularization and decay of its orbit (Burns, 1972; Yoder, 1982). However, the mechanism is ineffective for Deimos, most likely never below the synchronous orbit of Mars.

The near-circular and low-inclination orbits may rather suggest in situ formations (Goldreich, 1965), from either a proto-Martian or a postimpact debris disk (Canup & Salmon, 2018; Craddock, 2011; Rosenblatt et al., 2016). Another direct indication of the accretive origin is the bulk densities of Phobos and Deimos, at 1.86 and 1.47 g/cm$^3$, respectively (Andert et al., 2010; Jacobson, 2010), far lower than those of meteoritic analogs (Rosenblatt, 2011). The densities likely indicate significant porosities of the body accreted through gentle collisions governed by mutual gravitation (Richardson et al., 2002). Apart from self gravitation and bulk rotation of the debris cloud, the accretion could have been perceptibly influenced by tides raised by the primary body. Note that magnitude of the tidal and centrifugal potentials attenuates fast with $r_M^{-3}$, with $r_M$ being the distance to the primary (Soter & Harris, 1977).

The best fitting ellipsoid of Phobos measures approximately $13 \times 11.4 \times 9.1$ km$^3$ in semiaxes (Duxbury, 1989; Thomas, 1993; Willner et al., 2014), with the semimajor axis aligned toward Mars as a result of tidal locking (Figure 1). Various studies have suggested that tidal effects in the accretion process might be responsible for such triaxial shape (Rosenblatt & Charnoz, 2012; Soter & Harris, 1977), which may represent an equipotential figure of equilibrium. At a time when its density was largely unknown, Soter and Harris (1977) estimated that Phobos would be close to hydrostatic equilibrium near 3.5 Mars radii assuming a homogeneous interior with a density of 2 g/cm$^3$ (Chandrasekhar, 1969). Here we present an updated and independent analysis of Phobos' equilibrium form, using a refined density estimate and detailed shape model (though still assuming homogeneity). We establish an equipotential ellipsoid that serves as a natural reference level for measuring surface heights on Phobos. We examine two height statistics in order to quantify the degree of topographic

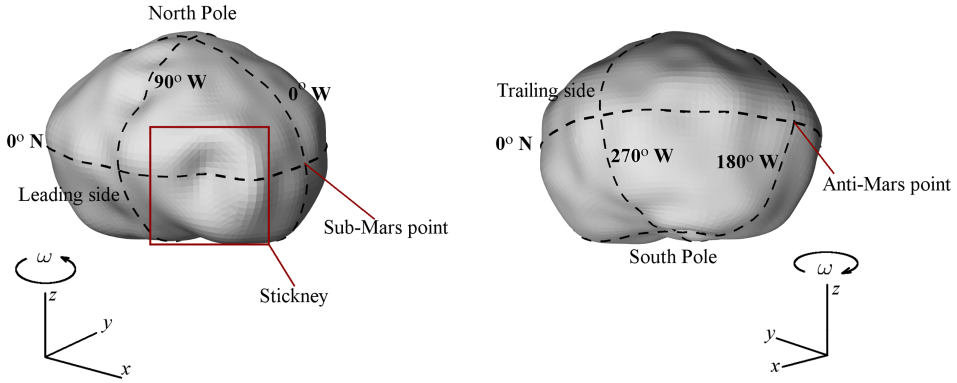


**Figure 1.** Shape, coordinate system of Phobos, and body orientation annotated with respect to its orbit around Mars. The largest crater, Stickney, is highlighted in the red rectangle.

equilibrium, which are strongly affected by Martian tides and, thus, distance from Mars. We discuss the implications of the results in connection with state of the art formulation models.

## 2. Normal Ellipsoid and Ellipsoidal Height of Phobos

To determine the equipotential ellipsoid of Phobos, we approximated its self gravitation by that of a polyhedral shape with a uniform bulk density and took into account centrifugal and tidal effects (see Supporting Information S1). Notably, the tidal force maximizes around the sub- and anti-Mars points along the major axis where it counteracts more than 20% of gravitation at the current distance of 2.76 Mars radii (Scheeres et al., 2019; Shi et al., 2016). Accordingly, the total potential over Phobos' surface displays a distinct tidal pattern that accounts for about 30% of the maxima (Figure 2a). We consider the gravity potential to comprise two distinct components (Hu, 2017),

$$W = U + \delta W, \tag{1}$$

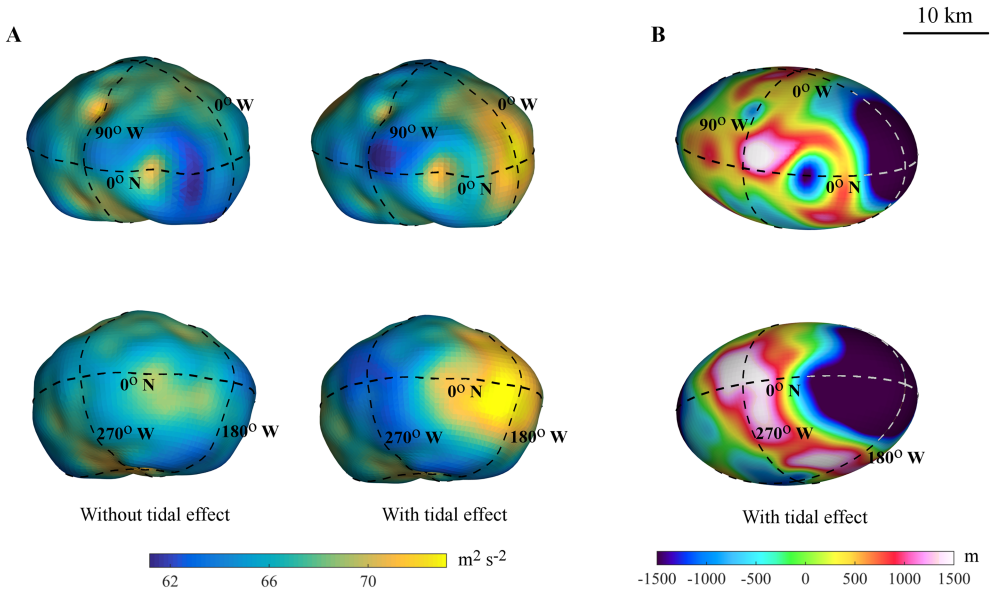


**Figure 2.** Gravity potential over the body surface and the normal ellipsoid of Phobos at the current distance of 2.76 Mars radii. The potential is color-coded on the shape in two complementary views (a). The tidal effect is distinguished by the comparison between a tide-free example (left column) and the actual, tidal case (right column). The ellipsoidal heights of the surface are measured from the normal ellipsoid (B). The negative heights in the sub- and anti-Mars regions correspond to the high surface potentials and are caused by tidal elongation of the normal ellipsoid. The coordinate system here is as in Willner et al. (2014).

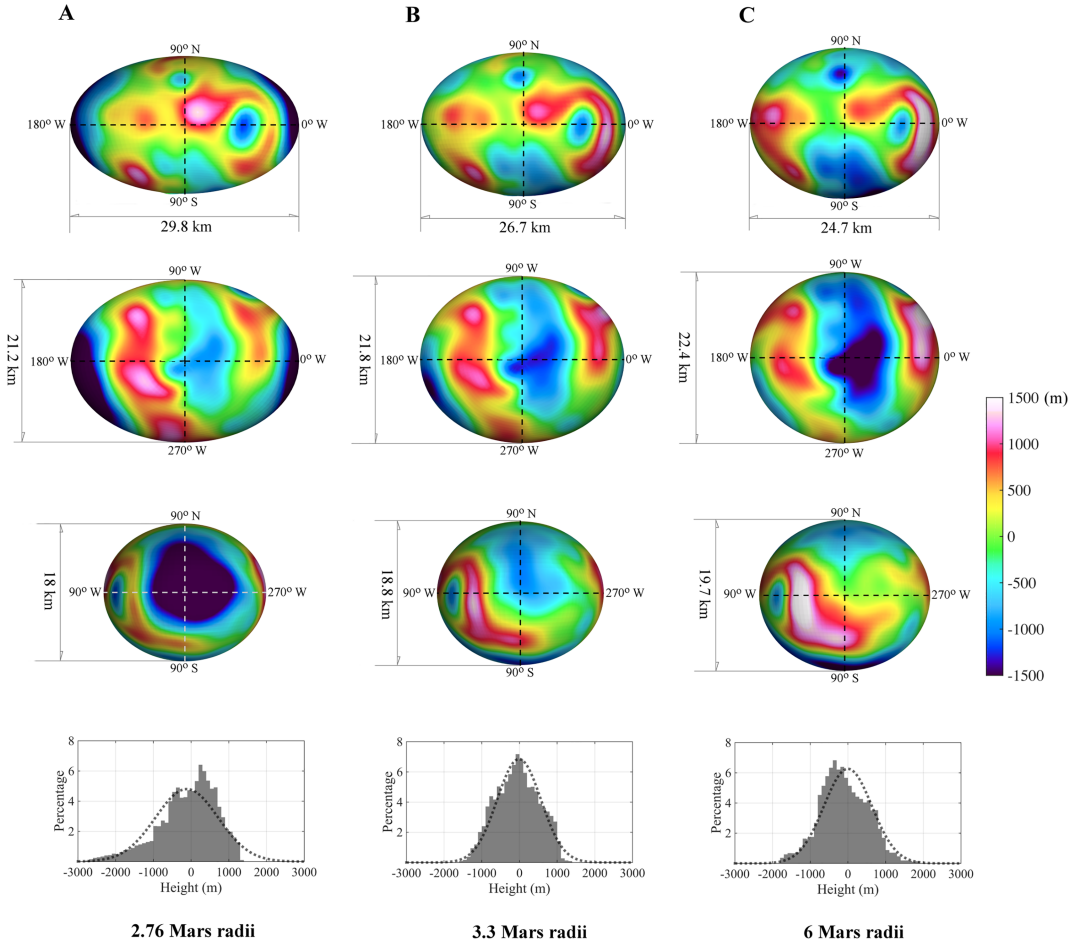


**Figure 3.** Heights on Phobos projected onto normal ellipsoid and histograms of height distribution at 2.76, 3.3, and 6.0 Mars radii. The three views are from the leading side (top row), the South Pole (second row), and sub-Mars point (third row). Gaussian distribution for the derived mean and standard deviation is indicated by dotted gray curve in comparison with each histogram (bottom row). (a) At 2.76 Mars radii, extreme negative heights of lower than −1,500 m ($2\sigma$) occur around the sub- and anti-Mars points, causing the distribution to be heavily left tailed. The distribution peaks at about 500 m. (b) The height undulation is moderated at 3.3 Mars radii; the distribution is nearly Gaussian and peaks near zero. (c) At 6 Mars radii, extreme heights, both positive and negative, are present around the sub-Mars and the South Pole. The distribution becomes asymmetric again and peaks around −500 m.

where $U$ represents a dominant, normal component caused by the polar and the equatorial flattenings of the body mass and $\delta W$ corresponds to small, residual disturbances. In the case of Phobos, $\delta W$ does not exceed 5% of the total potential. We solve for the equipotential surface in the form of an ellipsoid that generates $U$ (see Supporting Information S2). For a certain potential value, there exists a unique, corresponding equipotential ellipsoid. Of particular interest is the "normal ellipsoid" that corresponds to the average potential over the surface, which represents the equilibrium form of the body. This concept is well established for Earth and other terrestrial planets (Heiskanen & Moritz, 1967). The topographic variation beside the body ellipsoidicity affects the shape of the normal ellipsoid by about 1% (Supporting Information S3).

The dimensions of the normal ellipsoid for Phobos at the current distance are found to be 14.9 × 10.6 × 8.99 $km^3$. The higher elongation than the actual shape makes the sub- and anti-Mars sides the lowest places on Phobos at some 2 km below, as was also found in previous studies (Dobrovolskis & Burns, 1980). More rigorously, we measured the ellipsoidal heights as deviation of the topography from the normal ellipsoid along orthogonal directions. The heights are projected onto the normal ellipsoid (Figure 2b). Other than the few most prominent features, such as Stickney crater (see Figure 1), which can be identified as local minima, there is little correlation between the ellipsoidal heights and topography on Phobos. Instead, the height pattern is distinguished by a globally symmetric variation from extreme depths on the sub- and anti-Mars

sides to kilometer high plateaus on the leading and trailing sides. The root mean square (RMS) of heights over the entire surface is 830 m. Hence, the vast areas at depths of more than twice the RMS are clearly unequilibrated subject to strong tidal forces. Another obvious signature of disequilibrium is the asymmetric distribution of surface heights. As shown in Figure 3a, the height distribution on Phobos peaks at about 200 m but tends strongly toward negative heights. The pronounced tail is dominated by maximum depths over the sub- and anti-Mars regions.

## 3. Height Statistics in Higher Orbits

We performed calculations for various higher orbits, which Phobos had probably once occupied. We noted a steady decrease of the height RMS with increasing distance. At 3.3 Mars radii, the tidal force attenuates to about 50% of the current magnitude. Accordingly, the normal ellipsoid is $13.4 \times 10.9 \times 9.4$ km$^3$, visibly relaxed from that at 2.76 Mars radii (Figure 3b). The height RMS is reduced to 580 m, indicating better approximation of the normal ellipsoid to the actual figure of Phobos. The surface heights vary more evenly with extreme heights beyond 1,200 m largely suppressed. The height distribution is nearly symmetric and unimodal, with an unambiguous peak around zero. The near-Gaussian attributes suggest that the topography becomes nearly equipotential at 3.3 Mars radii. The Gaussianity can be explained by a prevalent observation that the topography formation resembles a random process up to a certain wavelength (Sayles & Thomas, 1978). For Phobos, this maximum wavelength then approaches the global, ellipsoidal dimensions of the body, conceivably controlled by the accretion process. Over shorter distances, the topography is shaped by increasingly random physical processes, such that the additional undulations become surface roughness.

At further distances, the fit of the normal ellipsoid to the body shape deteriorates, and the symmetry of the height distribution eventually breaks down. At 6 Mars radii, for instance, the height RMS increases to 637 m. The peak of the distribution is offset to roughly −500 m (Figure 3c). These moderate depths are widely found in both hemispheres, caused by the contracted and more spherical shape of the normal ellipsoid under diminishing tidal and rotational effects (Figure S1 and Table S1). As a result, the eastern rim of Stickney near the sub-Mars region is elevated to be the highest area on Phobos, as opposed to being the deepest at the current 2.76 Mars radii. The asymmetry of the height distribution is overall reversed from the pattern at present (Figures 3a and 3c).

The asymmetry of height distribution can be measured formally by the skewness (see Supporting Information S4). The skewness of a perfect Gaussian distribution is zero. In the case of Phobos, the maximum occurs at 2.76 Mars radii, the lowest orbit considered here (Figure 4). The skewness drops off until 3.34 Mars radii, at which distance a clear-cut minimum of 0.005 is reached while the height distribution resembles Gaussian (Figure 3b). It then rises with increasing distance from Mars, ever more slowly evidently due to attenuating tidal influence. In comparison, the height RMS is minimized slightly further away at 3.55 Mars radii. However, the variation between 3.3 and 4 radii is shallow, and the minimum is hardly distinguished. As with the skewness, the curve rises and flattens outward, indicating less notable change of the normal ellipsoid as tidal effect weakens (Figure S1). Thus, the skewness and RMS of heights narrow the origin of Phobos into between 3.34 and 3.55 Mars radii, whereas the former seems to offer a less ambiguous identification.

## 4. Implications on Phobos' Evolution

The inferred accretion distance of Phobos has immediate consequences on its subsequent evolution and lifetime. At the current rate of descent, Phobos is expected to survive for less than 50 Myr before it is tidally disrupted into a debris ring (Black & Mittal, 2015). Far less certain is the age of the body. Crater statistics suggests that Phobos may be a few Gyr old (Schmedemann et al., 2014; Thomas & Veverka, 1980), comparable to the age of Mars. It makes it a curious coincidence for us to see Phobos in the final 1–2% of its long lifetime (Oberst et al., 2014). The estimate is inconsistent with boulder statistics near Stickney, suggesting a surface age younger than 500 Myr (Ramsley & Head, 2017). On the other hand, if formed near 3.3 Mars radii, Phobos would have descended to its current location within the past 80 Myr, quite comparable to its presumed remaining lifetime of 50 Myr. We suspect that the plethora of impacts during the accretion could have contributed to the overabundance of craters, resembling the result of a bombardment.

How plausible is it that Phobos is about 100 Myr old? The premise is the existence of a debris ring extending to 3.3 Mars radii at the time of accretion. This ring could have resulted from a late impact (Canup & Salmon,

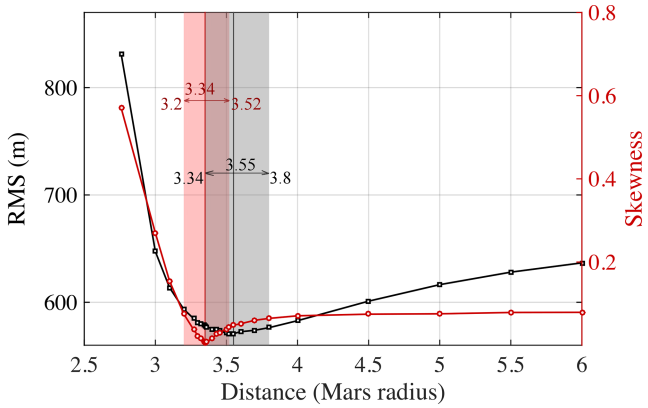


**Figure 4.** Topographic statistics of Phobos as function of distance to Mars. The RMS of height is indicated by the black curve with squared markers. The skewness of the distribution is shown by the red curve with circles. The shaded ranges correspond to an uncertainty of ±200 m in the semimajor axis of the normal ellipsoid.

2018; Craddock, 2011). Alternatively, it could be the aftermath of tidal disruption of an ancestor moon (Hesselbrock & Minton, 2017). Numerical simulations of ring dynamics revealed that, in such events, the ring mass is only partially lost via deposition onto Mars, whereas the remainder is driven upward and reaccretes outside the fluid Roche limit (at 3.1 Mars radii) (Hesselbrock & Minton, 2017). Thus, Phobos could be the descendent of a more massive ancestor, even after multiple ring-moon cycles. The equilibrium of Phobos at 3.3 Mars radii is in remarkable agreement with this scenario, which naturally explains the short life cycle of Phobos relative to the age of Mars.

The inferred accretion distance is valid if Phobos has not yet undergone appreciable deformation. This assumption might seem counterintuitive, particularly if Phobos had spent most of its lifetime inside the Roche limit. At present, the interior stress is dominated by gravitational pressure (Dobrovolskis, 1982). Assuming a commensurate rigidity above $10^6$ Pa (Hurford et al., 2016), the elastic tidal deformation of Phobos should not exceed tens of meters (Dobrovolskis, 1982). Before tidal forces eventually prevail near 2 Mars radii, any substantial deformations, for example, triggered by seismic events or the first episode of future disruption, would be of shear failure and manifested in surface faults not yet present on Phobos. The landslides identified on some crater walls are evidence of tidal deformation beginning on local scales (Shi et al., 2016). The surface slope distribution suggests Phobos has undergone erosion (Richardson & Bowling, 2014), which however should be restricted to the regolith layer less than 100 m in thickness (Thomas, 1993). The mean slope of about 11.5° meanwhile suggests that the topography is probably overall stable at the current distance (Richardson et al., 2019). Another intriguing case is the mesh of grooves. Their pattern does not indicate shear failure but rather alludes to tensile fracturing in a rigid crust overlying weaker interior deformed by about 20 m under tidal stress (Hurford et al., 2016). Hence, they could be shallow precursors of impending interior failure (Dobrovolskis, 1982).

Therefore, it is quite plausible the global triaxial dimensions of Phobos have not changed by more than 100 m during its orbital evolution. We recall that the numerical uncertainty of the normal ellipsoid derived from the shape model is smaller than 100 m (Supporting Information S3). The total uncertainty of less than 200 m encompasses a range of formation distance around the minima of height RMS and skewness, as depicted in Figure 4. Our independent results are consistent with the estimate by Soter and Harris (1977) within uncertainty.

## 5. Conclusion and Discussion

While much detail remains to be resolved by future missions to the Martian moons (Fujimoto et al., 2017), it is most likely that the moons have undergone divergent paths of evolution. Phobos may have long been broken up by tidal force of Mars but reaccreted, perhaps done so repeatedly (Hesselbrock & Minton, 2017). It is not least surprising that Phobos is observed in a low, fast-descending orbit before imminent tidal disruption. We believe that the cycle of breakup and accretion near the fluid Roche limit may have repeatedly produced triaxial objects. In other words, had it been observable, any predecessor of Phobos would have

exhibited triaxial shapes as Phobos itself. Work is currently underway to investigate in detail the figure of Deimos, which has probably always been outside the synchronous orbit under limited tidal influence.

**Acknowledgments**
We thank Dr. David Minton and an anonymous referee for critically reviewing the manuscript. The data in this analysis are publicly available from the project "Normal ellipsoid and ellipsoidal height of Phobos" archived on Open Science Framework (https://osf.io/ru3xq/). X. Hu has been supported by the Deutsche Forschungsgemeinschaft (DFG), Research Grant OB 124/14-1.

## References

Andert, T. P., Rosenblatt, P., Pätzold, M., Häusler, B., Dehant, V., Tyler, G. L., & Marty, J. C. (2010). Precise mass determination and the nature of Phobos. *Geophysical Research Letters*, *37*, L09202. https://doi.org/10.1029/2009GL041829

Black, B. A., & Mittal, T. (2015). The demise of Phobos and development of a Martian ring system. *Nature Geoscience*, *8*, 913–917. https://doi.org/10.1038/ngeo2583

Burns, J. A. (1972). Dynamical characteristics of Phobos and Deimos. *Reviews of Geophysics and Space Physics*, *10*, 463–483. https://doi.org/10.1029/RG010i002p00463

Burns, J. A. (1992). Contradictory clues as to the origin of the Martian moons. In H. H. Kieffer, B. M. Jakosky, C. W. Snyder, & M.S. Matthews (Eds.), *Mars* (pp. 1283–1301). Tucson: University of Arizona Press.

Canup, R., & Salmon, J. (2018). Origin of Phobos and Deimos by the impact of a Vesta-to-Ceres sized body with Mars. *Science Advances*, *4*(4), eaar6887. https://doi.org/10.1126/sciadv.aar6887

Chandrasekhar, S. (1969). *Ellipsoidal figures of equilibrium*, The Silliman Foundation Lectures. New Haven: Yale University Press.

Craddock, R. A. (2011). Are Phobos and Deimos the result of a giant impact? *Icarus*, *211*, 1150–1161. https://doi.org/10.1016/j.icarus.2010.10.023

Dobrovolskis, A. R. (1982). Internal stresses in PHOBOS and other triaxial bodies. *Icarus*, *52*, 136–148. https://doi.org/10.1016/0019-1035(82)90174-9

Dobrovolskis, A. R., & Burns, J. A. (1980). Life near the Roche limit—Behavior of ejecta from satellites close to planets. *Icarus*, *42*, 422–441. https://doi.org/10.1016/0019-1035(80)90105-0

Duxbury, T. C. (1989). The figure of PHOBOS. *Icarus*, *78*, 169–180. https://doi.org/10.1016/0019-1035(89)90075-4

Fujimoto, M., Miyamoto, H., & Kuramoto, K. (2017). JAXA's Martian Moons eXplortaion, MMX. *European Planetary Science Congress*, *11*, EPSC2017–136.

Goldreich, P. (1965). Inclination of satellite orbits about an oblate precessing planet. *The Astronomical Journal*, *70*, 5. https://doi.org/10.1086/109673

Heiskanen, W. A., & Moritz, H. (1967). *Physical geodesy*. San Francisco: W. H. Freeman.

Hesselbrock, A. J., & Minton, D. A. (2017). An ongoing satellite-ring cycle of Mars and the origins of Phobos and Deimos. *Nature Geoscience*, *10*(4), 266–269. https://doi.org/10.1038/ngeo2916

Hu, X. (2017). Normal gravity fields and equipotential ellipsoids of small objects in the solar system: A closed-form solution in ellipsoidal harmonics up to the second degree. *The Astrophysical Journal*, *850*(1), 107. https://doi.org/10.3847/1538-4357/aa9222

Hurford, T. A., Asphaug, E., Spitale, J. N., Hemingway, D., Rhoden, A. R., Henning, W. G., et al. (2016). Tidal disruption of Phobos as the cause of surface fractures. *Journal of Geophysical Research: Planets*, *121*, 1054–1065. https://doi.org/10.1002/2015JE004943

Jacobson, R. A. (2010). The orbits and masses of the Martian satellites and the libration of Phobos. *The Astronomical Journal*, *139*(2), 668–679. https://doi.org/10.1088/0004-6256/139/2/668

Lambeck, K. (1979). On the orbital evolution of the Martian satellites. *Journal of Geophysical Research*, *84*, 5651–5658. https://doi.org/10.1029/JB084iB10p05651

Oberst, J., Zakharov, A., & Schulz, R. (2014). Why study Phobos and Deimos? An introduction to the special issue. *Planetary and Space Science*, *102*, 1–1. https://doi.org/10.1016/j.pss.2014.05.010

Peale, S. J. (1999). Origin and evolution of the natural satellites. *Annual Review of Astronomy and Astrophysics*, *37*, 533–602. https://doi.org/10.1146/annurev.astro.37.1.533

Pieters, C. M., Murchie, S., Thomas, N., & Britt, D. (2014). Composition of surface materials on the moons of Mars. *Planetary and Space Science*, *102*, 144–151. https://doi.org/10.1016/j.pss.2014.02.008

Ramsley, K. R., & Head, J. W. (2017). The Stickney Crater ejecta secondary impact crater spike on Phobos: Implications for the age of Stickney and the surface of Phobos. *Planetary and Space Science*, *138*, 7–24. https://doi.org/10.1016/j.pss.2017.02.004

Richardson, J. E., & Bowling, T. J. (2014). Investigating the combined effects of shape, density, and rotation on small body surface slopes and erosion rates. *Icarus*, *234*, 53–65. https://doi.org/10.1016/j.icarus.2014.02.015

Richardson, J. E., Graves, K. J., Harris, A. W., & Bowling, T. J. (2019). Small body shapes and spins reveal a prevailing state of maximum topographic stability. *Icarus*, *329*, 207–221. https://doi.org/10.1016/j.icarus.2019.03.027

Richardson, D. C., Leinhardt, Z. M., Melosh, H. J., Bottke, W. F., & Asphaug, E. (2002). Gravitational aggregates: Evidence and evolution. In Bottke, W. F., Cellino, A., Paolicchi, P., & Binzel, R. P. (Eds.), *Asteroids iii* (pp. 501–515). Tucson: University of Arizona Press.

Rosenblatt, P. (2011). The origin of the Martian moons revisited. *The Astronomy and Astrophysics Review*, *19*, 44. https://doi.org/10.1007/s00159-011-0044-6

Rosenblatt, P., & Charnoz, S. (2012). On the formation of the Martian moons from a circum-Martian accretion disk. *Icarus*, *221*, 806–815.

Rosenblatt, P., Charnoz, S., Dunseath, K. M., Terao-Dunseath, M., Trinh, A., Hyodo, R., et al. (2016). Accretion of Phobos and Deimos in an extended debris disc stirred by transient moons. *Nature Geoscience*, *9*(8), 581–583. https://doi.org/10.1038/ngeo2742

Sayles, R. S., & Thomas, T. R. (1978). Surface topography as a nonstationary random process. *Nature*, *271*, 431–434. https://doi.org/10.1038/271431a0

Scheeres, D. J., Van wal, S., Olikara, Z., & Baresi, N. (2019). Dynamics in the Phobos environment. *Advances in Space Research*, *63*(1), 476–495. https://doi.org/10.1016/j.asr.2018.10.016

Schmedemann, N., Michael, G. G., Ivanov, B. A., Murray, J. B., & Neukum, G. (2014). The age of Phobos and its largest crater, Stickney. *Planetary and Space Science*, *102*, 152–163. https://doi.org/10.1016/j.pss.2014.04.009

Shi, X., Oberst, J., & Willner, K. (2016). Mass wasting on Phobos triggered by an evolving tidal environment. *Geophysical Research Letters*, *43*, 12,371–12,379. https://doi.org/10.1002/2016GL071650

Soter, S., & Harris, A. (1977). The equilibrium figures of Phobos and other small bodies. *Icarus*, *30*(1), 192–199. https://doi.org/10.1016/0019-1035(77)90133-6

Thomas, P. C. (1993). Gravity, tides, and topography on small satellites and asteroids: Application to surface features of the Martian satellites. *Icarus*, *105*(2), 326–344. https://doi.org/10.1006/icar.1993.1130

Thomas, P. C., & Veverka, J. (1980). Crater densities on the satellites of Mars. *Icarus*, *41*(3), 365–380. https://doi.org/10.1016/0019-1035(80)90221-3

Willner, K., Shi, X., & Oberst, J. (2014). Phobos' shape and topography models. *Planetary and Space Science*, *102*, 51–59. https://doi.org/10.1016/j.pss.2013.12.006
Yoder, C. F. (1982). Tidal rigidity of phobos. *Icarus*, *49*(3), 327–346. https://doi.org/10.1016/0019-1035(82)90040-9